Fluence-dependent dynamics of localized excited species in monolayer versus bulk MoS_2

Tim Völzer, Franziska Fennel, Tobias Korn, and Stefan Lochbrunner*
Institute of Physics and Department "Life, Light & Matter," University of Rostock, 18059 Rostock, Germany

(Received 11 March 2020; accepted 4 January 2021; published 20 January 2021)

Transition-metal dichalcogenides are characterized by a layered lattice structure, facilitating the fabrication of two-dimensional crystals. Concerning their electronic properties, these monolayers differ fundamentally from the bulk material, exhibiting direct band gaps and significantly higher exciton binding energies. Hence, to shed light on how the crystal thickness influences the relevant excited states and in particular their dynamics, we performed time-resolved optical pump-probe spectroscopy on monolayer and bulk samples of molybdenum disulfide (MoS_2) for a broad range of excitation fluences. The observed transient spectra result from photoinduced shifts in the band structure. Here, we find evidence for a localized nature of the excited species as opposed to the common model of band-gap renormalization. At high excitation densities, strong collisional broadening of the shifted absorption occurs. Within the first picosecond after excitation, the free carriers thermalize, while in the monolayer, additionally, electrons and holes pair to form excitons. On longer time scales up to several nanoseconds, the excited populations decay. In the bulk sample, the corresponding signal reduction could be described in terms of a defect-assisted Auger recombination of electrons and holes. For monolayer MoS_2, in contrast, two-dimensional diffusion leads to recombination of the excitons at defect sites.

DOI: 10.1103/PhysRevB.103.045423

I. INTRODUCTION

Transition-metal dichalcogenides (TMDCs) have emerged as two-dimensional (2D) materials, as their layered structure with weak van der Waals interlayer forces facilitates the fabrication of atomically thin crystals. Here, the limiting case of a triatomic monolayer (1L) differs decisively from the bulk, exhibiting drastically enhanced exciton binding energies and a direct band gap [1–4], i.e., resulting in a pronounced rise of the photoluminescence (PL) [5,6].

Apart from these fundamental issues, these thin films have raised particular interest in view of various applications [7]. Generally, as a consequence of the strong light-matter interactions in TMDCs, they are predestined for optoelectronics such as light-emitting diodes [8] and phototransistors [9]. In the field of photodetectors, developments towards high responsivities [10] and ultrafast response times [11] have been pursued. In the latter case, short carrier diffusion pathways in atomically thin layers allow for a fast charge separation after exciton dissociation. Yet, these processes compete with loss mechanisms, such as trapping and recombination, lowering the quantum efficiency of the devices [10].

Furthermore, especially in molybdenum and tungsten disulfides (MoS_2 and WS_2, respectively), the energy of the conduction-band (CB) minimum matches the redox potential of the hydrogen evolution reaction (HER) in the process of water splitting [12]. Hence, these materials constitute promising HER photo- [13–15] and electrocatalysts [16,17]. Here, the crystal edges have been identified as the catalytically active sites [12], thus making thin and small flakes preferable catalytic systems, owing to their high specific surfaces or active center densities. On the downside, this location of the sites causes the (quantum) efficiency of the catalytic reaction to depend critically on an undisturbed, low-loss transport of excitation energy or excited species through the material to the edges [14,15,18], similar to the situation in (opto)electronics.

All in all, this demonstrates the importance of excited species dynamics for applying TMDCs in the aforementioned technologies. Considering the impact of thickness on their electronic properties, we expect distinct behaviors for the 1L and the bulk. Common approaches for investigating the excited species' ultrafast dynamics are transient absorption or reflectance spectroscopy, which have been performed by various groups on mono- and few-layer [19–26] as well as on bulk [20,27–29] flakes of different TMDCs. The obtained signals or spectra bear striking similarities in most studies; however, their evaluations and interpretations concerning the physical origin of the signatures strongly differ. Here, various excitonic effects [19,23,27] and band filling [20,28] were considered, although the model of band-gap renormalization (BGR) [19,21,24] has gained broader acceptance lately. Likewise, various processes governing the dynamics and decay of the signals are discussed, yet there are fundamental differences between these studies regarding sample quality and thickness, excitation fluence regime, and probe wavelength. In our view, systematic variation of the excitation density should allow for a better characterization of the excited species and resolve some of the contradicting interpretations. With this goal in mind, we studied the light-induced dynamics in 1L and bulk MoS_2 in dependence on the excitation fluence and developed a physical model resulting in a consistent interpretation of the time-resolved dynamics.

In this work, we present all optical pump-probe [30] measurements of 1L and bulk MoS_2, exciting with a wavelength of 400 nm and probing the whole visible range with a white light continuum. In particular, the dynamics are analyzed with respect to their dependence on the excitation fluence, providing

*stefan.lochbrunner@uni-rostock.de

insights into the nature of the excited species. Thus, we can trace and separate decay mechanisms that behave nonlinearly with respect to the excitation density or nonexponentially with time. Careful analysis of the transient spectra is performed by globally fitting the transient spectra to discriminate different signatures, such as shifts, broadenings, and decays, to associate the spectral features to the underlying mechanisms. In the course of this, we find subtle contradictions to the common BGR model, especially to the predicted peak shift with increasing density of the excited species. Hence, we propose a picture of localized species, which cause spatially limited distortions of the lattice and the respective energy bands.

II. RESULTS AND DISCUSSION

A. Preparation and identification of monolayer MoS_2 flakes

We fabricated atomically thin films on a polydimethylsiloxane (PDMS) substrate, following the advanced exfoliation approach developed by Castellanos-Gomez *et al.* [31,32]. We scanned for and selected promising flakes via optical microscopy. A monolayer area was identified based on its transmission contrast [33–35] and PL [5,6]. As a bulk sample for comparison, we selected a crystal of several tens of nanometers of vertical extent. The details of the sample preparation and thickness determination for both samples are given in Secs. I and II of the Supplemental Material (SM) [36], respectively.

The absorption spectra in the visible range of the monolayer and bulk samples feature the same three prominent peaks(see Fig. 1). The lower energetic peaks A and B at about 650 and 600 nm, respectively, correspond to excitonic transitions located at the *K* point [37,38], while the energetically broader and higher contribution C near 450 nm can be assigned to band nesting in different regions of the Brillouin zone, especially in the environment of the Γ point [38–40]. For the A and C peaks, we note a blueshift from bulk to monolayer, as has previously been observed for dry as well as liquid-phase exfoliated flakes [24,37].

B. Transient band shifts induced by localized excited species

We now turn to the transient absorption spectra $\Delta A(\lambda, t)$, which were obtained by pump-probe spectroscopy with a time resolution of 100 fs. Details of the experimental setup are presented in the SM, Sec. III [36]. All measurements were performed under ambient conditions. Despite the difference in the C transition energies between monolayer and bulk MoS_2, the high excess energy of the 400-nm pump pulses with respect to this absorption band suggests the excitation of free charge carriers in several parts of the Brillouin zone in both cases.

When comparing the transient spectra of bulk and monolayer MoS_2, as shown in Figs. 1(a) and 1(b), respectively, one finds strikingly similar patterns in both cases: Negative ΔA peaks (A^- and B^-) at the positions of the original static absorption bands A and B are accompanied by redshifted positive features (A^+ and B^+) [24,40], suggesting a photoinduced shift of the absorption to lower energies. Accordingly, each pair of positive and negative peaks resembles a single process, namely, the shift of the original, static absorption peak. These

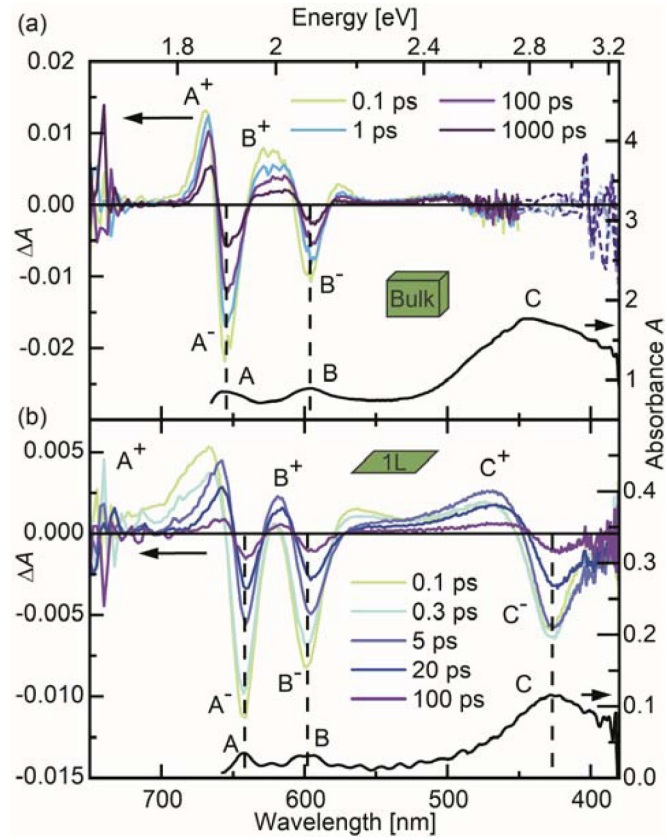

FIG. 1. (a) Bulk and (b) monolayer static absorption (black lines) and transient spectra (colored lines) for an excitation fluence of 31 μJ/cm^2 at various probe delays. The negative transient peaks match the static absorption peaks, as indicated by the dashed vertical lines. Each of these transient signatures is accompanied by a corresponding redshifted, positive feature. For the monolayer, these peaks appear broader than in the bulk case and an additional peak pair arises around the wavelength of the C absorption. The dashed curves in (a) indicate a region of high noise and are therefore smoothed.

observations are consistent with the results of our previous work [29], where we excited a bulk sample at 665 nm. Consequently, the shift is caused by the excited species irrespective of their exact location in the band structure.

With reference to the underlying mechanism for this shift in the bulk, we already discussed a variety of possible explanations in that earlier study. Here, we expand this discussion to the single layer. Considering the similarity of the bulk and monolayer spectra, despite the enormous difference in exciton binding energy, excitonic effects such as trion or biexciton formation seem highly improbable as the origin of the shift. The intensely discussed approach of band-gap renormalization [19–21,24,41], on the contrary, provides the benefit of being equally applicable to crystals of every thickness. Pogna *et al.* obtained transient spectra in 1L MoS_2 similar to ours and explained them mostly with BGR [22]. In this picture, the different charge distribution of the excited species compared to the ground state affects the band structure and shifts the band levels and likewise the absorption peaks. However, as the carriers are regarded as completely delocalized over the whole crystal, the magnitude of the redshift directly depends on the excited carrier density [42].

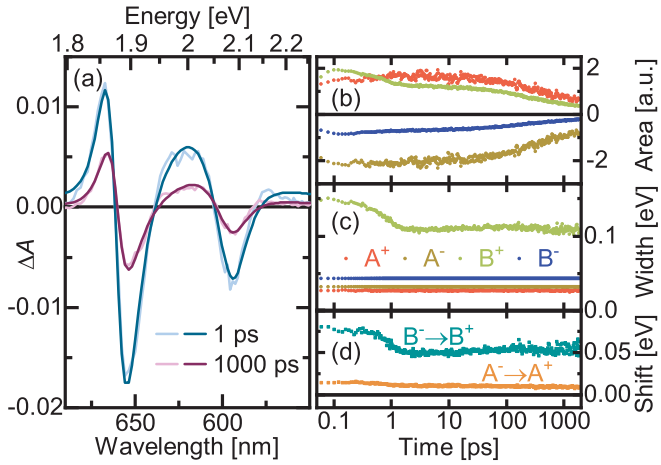

FIG. 2. Lorentzian peak fitting of the $A^{\pm}$ and $B^{\pm}$ features in the transient spectra for the bulk sample excited with a fluence of 31 $\mu J/cm^2$. (a) Measured and fitted transient absorption spectra at different probe delays. Bright lines represent the data and dark lines stand for the fits, showing a good agreement between the two. (b) Temporal evolution of the areas of the four Lorentz peaks. All curves clearly decrease in amplitude. (c) Time-resolved peak widths. The B^- width decreases within the first few picoseconds, while all other features exhibit constant values. (d) Peak shift magnitude from negative to positive contribution for the A and B pair over time. The shift is reduced during the first few picoseconds and does not change afterwards.

To probe the applicability of this model to our data, we fitted the transient spectra by a sum of four Lorentzian profiles in the range of the $A^{\pm}$ and $B^{\pm}$ peaks to distinguish between a shift of the positive peaks' positions and a mere reduction of the peak areas, as the excited species density decreases over time. As the negative features originate from the static absorption, we fixed their center energy and width to reduce the number of free parameters. The respective values were extracted from the static absorption spectra, as depicted in Fig. 1. The resulting fits, which match the data well, as well as the time evolution of the obtained parameter are presented in Fig. 2. The extracted parameters demonstrate that the long-term decay of the signal corresponds to merely a reduction of the peak area, whereas the shift, i.e., the center position difference between negative and positive peaks, remains constant. Fittings performed for higher excitation fluences and for the monolayer, as well as results obtained by using another line-shape function, can be found in Sec. IV of the SM [36]. Despite a higher noise and interfering additional spectral signatures, they reproduce the tendency that the dynamics are determined by the evolution of the peak area rather than that of the shift. These findings contradict the model of BGR resulting from delocalized excited species. Since our data mainly describe a shrinkage of the transient peaks with decaying excited populations instead of shifts, we propose a rather localized nature of the excited species. In this case, the locally altered charge distribution interacts with the band structure, leading to a new equilibrated electronic structure with a shifted absorption. Here, a higher number of excited species only causes a larger fraction of the crystal volume to be affected by the shift in absorption, but it does not change the spectral magnitude of the shift. A possible explanation for the localization could be the formation of polarons. These quasiparticles are commonly understood as carriers inducing deformation of the lattice and the charge distribution in their vicinity and traveling together with the potential dip that is caused by their own presence [43]. This interpretation would explain the local nature of the excited species, as Holstein polarons typically extend over about one unit cell. Furthermore, this picture intrinsically contains energy shifts in terms of the potential dip, accounting for the signatures in the transient spectra. Polarons have already been observed in surface-doped 1L MoS_2, causing energy shifts of several tens of meV [44]. Likewise, theoretical studies predict similar mechanisms and shifts for excitonic polarons in monolayer TMDCs [45]. Thus, this concept can be generally applied to free carriers as well as excitons independent of the crystal thickness.

In spite of their similarities, the spectra of the two samples differ from each other in two aspects: First, in the 1L MoS_2, we clearly observe an additional pair of a positive and negative peak, denoted as C^+ and C^-, corresponding to the C absorption band, while comparable signatures barely stand out from the noise in the bulk spectra. This can be explained by the larger width of the static C absorption peak in the thick crystal compared to the monolayer, making it less sensitive to shifts. As a second point, we note that the positive transient signals in the thinner sample appear significantly broader than their bulk counterparts. This enlarged width can be interpreted in terms of a collisional broadening as a consequence of Coulomb scattering of the excited species [19,23,28]. In the bulk, the Coulomb potential is screened more effectively [1,41] and the successive absorption of pump fluence during propagation through the sample leads to a lower average excited carrier density, resulting in a less pronounced broadening than in the monolayer. In the latter, however, the positive peaks A^+ and B^+ strongly overlap and partially cancel out with the negative signals A^- and B^-, causing the B^+ contribution to seemingly almost vanish.

The temporal evolution of the transient spectra for both samples is split into two major regimes on the (sub)picosecond and subnanosecond time scale. In the bulk, the fast dynamics manifest as a slight decrease of the transient amplitude and an apparent blueshift of the peak maximum at A^+. As the fit results in Fig. 2 prove, this is caused by a partial reduction of the photoinduced redshift and by narrowing of the positive peaks.

Generally, these fast processes are associated with the thermalization of excited carriers [24,27,29]. On a closer look, however, one has to distinguish between two separate effects. First, the carriers excited to high-lying regions of the CB rapidly relax into their respective band minimum or maximum by carrier-carrier scattering [46], as reported by time- and angle-resolved photoelectron spectroscopy (trARPES) [39,47]. Since this process takes place within 50–100 fs, we are not able to resolve it in our measurements. After this relaxation into the band extremum, the carriers follow a thermal distribution with an extremely high temperature, corresponding to their excess energy. From there on, carrier-phonon interaction dissipates this energy as heat to the crystal lattice. We attribute the picosecond-time-scale dynamics to

this process. As the excited species and the lattice equilibrate, the former cool down, reducing collisional broadening and therefore narrowing the positive peaks [see Fig. 2(c)]. Additionally, the reduced shift that occurs on this time span in Fig. 2(d) shows that cooled excited carriers disturb the local charge distribution and in turn alter the band structure less strongly than hot ones.

In the monolayer, a closer look especially at the A^+ peak in Fig. 1(b) reveals a further distinction of the thermalization component. First, on a time scale of several hundred femtoseconds, a signal reduction occurs, somewhat faster than, yet comparable to, the cooling times observed in the bulk. We interpret this as a proceeding localization of the excited carriers. In a local picture, a hot carrier will be characterized by a spatially smeared-out charge distribution that barely adapts to the local potential. Upon losing their excess energy, however, the particles will accumulate in local energy minima. This localization leads to a reduced affected crystal volume and, thus, a lower transient signal amplitude results as observed. Afterwards, within several picoseconds, we register a notable decrease of the collisional broadening, as the positive peaks narrow and rise in amplitude (see SM, Fig, S6 [36]). We interpret this as an evidence for exciton formation from thermalized carriers, as a consequence of the high exciton binding energy in the monolayer [48]. In the initial electron-hole plasma, the carriers move independently, each surrounded by their (dielectrically screened) Coulomb potential, despite an overall charge neutrality. When electron and hole form a bound pair, though, their charges compensate, reducing their Coulomb-scattering cross sections. Simultaneously, the excited particle density halves; hence, collisional broadening weakens and the positive transient peaks narrow.

As the second part of the dynamics, we observe the decay of the spectra on a subnanosecond time scale. Here, the recombination of electrons and holes (respectively, excitons) takes place. Irrespective of the sample thickness, the signal at all characteristic peaks decays at the same rate (see Sec. V of the SM [36]) and the spectral shape remains constant. This provides another evidence that the (thermalized) excited species density merely influences the amplitude of the transient peaks, while their positions do not change. In other words, with fewer excited species present, the photoinduced redshift of the static absorption affects a smaller fraction of the crystal volume, yet the absorption is shifted by the same amount of energy. Consequently, we can take the transient signal amplitude as a measure for the excited species density. A comprehensive analysis of their recombination mechanisms is presented in Sec. II D.

C. Density-dependent peak broadening and saturable absorption

To gain insight into the detailed nature of the decay dynamics, we vary the pump fluence searching for indications of nonlinear multiparticle processes. With an increase of the pump fluence, the transient spectra of both bulk and monolayer MoS_2 experience a sublinear amplitude growth as well as a further broadening of the positive peaks, as can be noted in Fig. 3. The latter results from the higher density of excited species, delivering more potential scattering partners, ergo stronger collisional broadening.

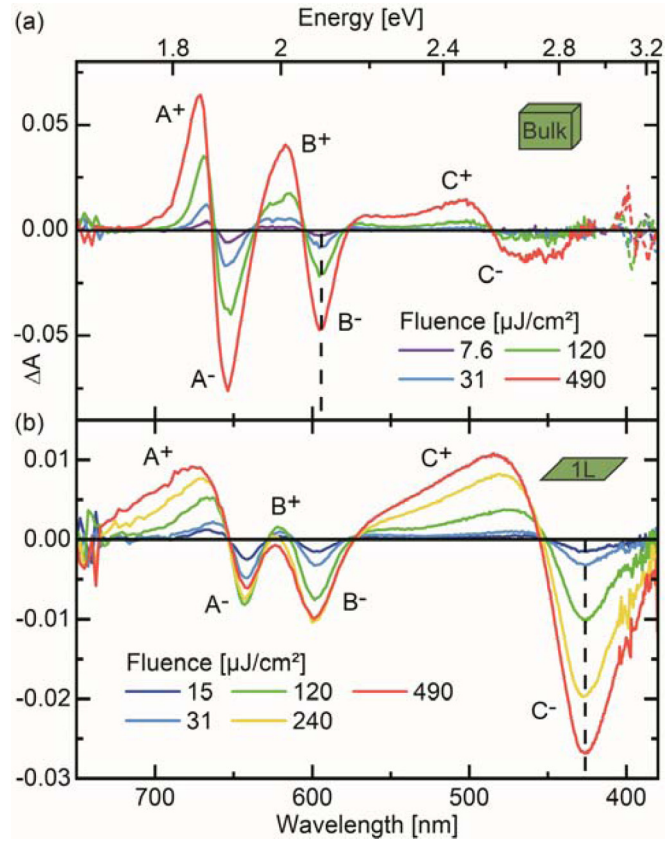

FIG. 3. (a) Bulk and (b) monolayer transient spectra at a probe delay of 1 ps for different pump fluences. The dashed lines mark the wavelengths considered for the analysis of the signal dynamics in the following sections. (a) The spectral shape remains essentially constant, with the amplitude increasing with fluence. The dashed curves indicate a region of high noise and are therefore smoothed. (b) The positive contributions broaden, and some stagnate or shrink, distorting the shape at high intensities.

In the bulk, one notices this effect most clearly for the A^+ peak [Fig. 3(a)]. Moreover, the peak heights increase sublinearly with pump fluence, indicating a saturated absorption behavior [29,49]. Yet, all four contributions related to the A and B peaks exhibit equal decay curves even at the highest fluence (see SM, Fig. S7(b) [36]), suggesting the signals to directly represent the excited carrier density. In accordance with previous studies [29], we chose the B^- peak at 596 nm for a detailed analysis of the bulk decay dynamics. The results of the fittings, in contrast, are not suitable for this purpose, since they should only be regarded qualitatively, as discussed in detail in Sec. IV of the SM [36].

In the monolayer, however, due to the weakened screening, collisional broadening is significantly more prominent, as can be seen in Fig. 3(b). Here, the $A^\pm$ and $B^\pm$ features overlap so strongly that the spectral shape is drastically distorted and the relation between excitation density and transient signal deviates significantly from a linear or even monotonic behavior in the corresponding wavelength region. As the peak fitting procedure yielded no results in case of high fluences(see Sec. IV of the SM [36]), we also cannot analyze peak areas as a measure for the exciton density. Therefore, we chose the C^- peak at 427 nm for a detailed investigation of the decay dynamics.

As the excitons induce a shift of the complete absorption, they cause the C^- contribution despite being located around the band minima. Here, the signal amplitude grows linearly with pump fluence, suggesting that it directly represents the exciton density. The sole exception from this behavior is observed for the highest intensity. Here, however, a saturation of the absorption similar to the bulk might come into play. In addition to this, the exciton density of up to 2×10^{14} cm^{-2} for the highest excitation fluence approaches the range of the Mott density in the order of 10^{14} cm^{-2}, as follows from an exciton Bohr radius of roughly 1 nm [1,4,19,38]. In this regime, the lattice is (spatially) saturated with excitons, causing a stagnation of the transient signal strength. In the extreme case of drastically higher excited species densities compared to our work, Chernikov *et al.* even observed an almost complete bleaching of the (shifted) absorption after excitation of WS_2 monolayers [19].

D. Auger recombination and diffusion-limited exciton trapping

To shed light on the underlying mechanisms for the excited species recombination in monolayer and bulk, we compare time traces at characteristic wavelengths for various pump fluences. Following their linear density dependence, as discussed in the previous section, we selected time traces of the B^- feature at 596 nm for the bulk and of the C^- peak at 427 nm for the monolayer sample. In Fig. 4, we compare the traces normalized to their value after the initial thermalization to find indications for multiparticle processes.

For the bulk material, we find a distinct acceleration of the signal decay with growing fluence, pointing to a quadratic dependence of the rate on the carrier density, as for the recombination of an electron from the conduction band with a hole from the valence band (VB). On top of that, we observe a counterintuitive phenomenon at the long-term tails of the high-fluence traces: For a quadratic recombination rate, a curve normalized to its starting value will decay faster the higher the initial signal or population. Nevertheless, the decay for the highest excitation density [red curve in Fig. 4(a)] falls behind the one for the next-lower fluence [green curve in Fig. 4(a)] for a time delay larger than 1000 ps. This may be explained by the involvement of a third species that catalyzes the recombination. If a significant fraction of this species is occupied when large numbers of carriers recombine, the signal decay will be slowed down. Such a behavior may be caused by defects, which mediate the recombination yet become inactive when occupied. The characteristics of these dynamics can be described by the model of defect-assisted Auger recombination [25,26,29,40,49,50]. Correspondingly, we fitted the time traces in terms of the following differential equation, describing the trapping of a free electron at a defect site via Auger scattering with another CB electron:

$$\frac{dn_e}{dt} = -\frac{dn_d^*}{dt} = -k_A n_e^2 (n_{d,0} - n_d^*(t)),$$
$$n_d^*(0) = 0,\ n_e(0) = n_0, \qquad (1)$$

with $n_e(t)$ and $n_d^*(t)$ being the time-dependent volume densities of free electrons and occupied defects, respectively, k_A the Auger rate constant, as well as $n_{d,0}$ and n_0 the overall available defect density and the initially excited electron density,

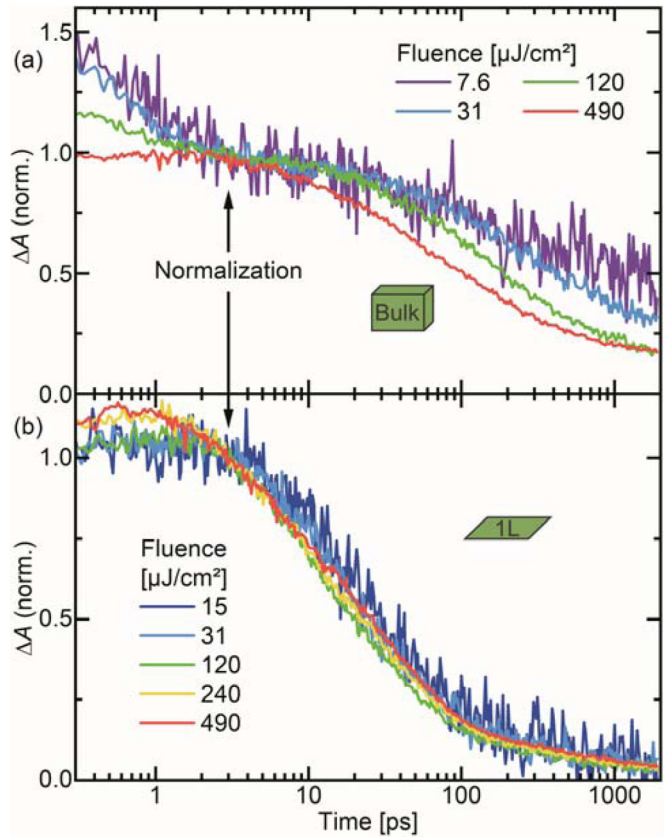

FIG. 4. Normalized time traces for various pump fluences at characteristic peak wavelengths, as indicated in Fig. 3, for (a) bulk at 596 nm and (b) monolayer at 427 nm. The arrows mark the time points used for the normalization. (a) Generally, the decay proceeds faster with increasing fluence. Yet, the green and red lines intersect at longer times. (b) The curves exhibit almost identical shape, independent of the applied pump fluence.

respectively. The second step of the Auger model, namely, the recombination of a trapped electron and a VB hole, turned out to exceed the experimental time range and was not fitted. Nevertheless, we accounted for amplitude contributions of holes or occupied defects. The measured and fitted curves are displayed in Fig. 5(a), showing an excellent agreement and yielding a trapping rate of $k_A \approx 10^{-30}$ cm^6 s^{-1}, and an overall defect density of $n_{d,0} \approx 10^{20}$ cm^{-3}. Additionally, we found a weak signature of holes and defects associated with $n_d^*(t)$, making up roughly 10% of the total amplitude. These extracted parameters bear a strong resemblance to those obtained for bulk MoS_2 excited at 665 nm [29], confirming that the recombination does not depend significantly on the excitation wavelength.

For the monolayer, in contrast to the bulk, the normalized time traces in Fig. 4(b) show virtually identical shapes, exhibiting hardly any fluence dependence. This behavior indicates a decay rate depending linearly on the exciton density and allows to exclude excitation density-dependent decay mechanisms like exciton-exciton annihilation for the monolayer. Yet, defects are still expected to play an important role as traps in the recombination [25], especially since they are particularly located at the crystal surface [26]. As a decisive difference to the mobile, free carriers in the bulk, we suppose

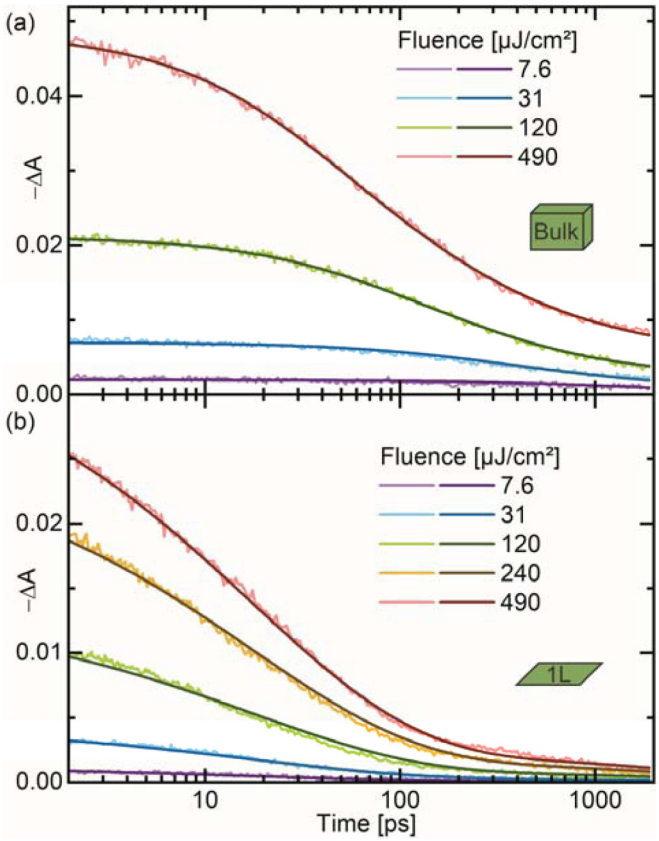

FIG. 5. Fitted decay dynamics for (a) bulk and (b) monolayer. Pale colors indicate the experimental data at the wavelengths indicated in Fig. 3, while dark shaded lines represent the fit. Both diagrams demonstrate a good agreement between the measurement and the fit.

the excitons in 1L MoS_2 exhibit a much lower mobility, owing to their bound nature. Consequently, we propose a trapping of excitons at defect sites, with a temporal evolution governed by the diffusion of the excitons towards the spatially fixed, randomly distributed traps [51]. The time dependence of such a diffusion-limited decay in d dimensions has been solved in theoretical studies, yielding a stretched exponential decay of the diffusive particle density $n(t)$ [52,53]:

$$n(t) \propto \exp(-Bt^{\frac{d}{d+2}}),$$
$$B = c n_t^{\frac{2}{d+2}} D^{\frac{d}{d+2}}, \tag{2}$$

with the diffusion coefficient D and the static trap density n_t. The numeric constant c depends on the dimensionality of the system, taking a value of $c = 8.525$ in a two-dimensional crystal [52].

An intuitive approach to understanding the origin of the stretched exponential is provided by the random spatial distribution of the defects. In regions with a high local trap density, the mean exciton diffusion pathway is short, resulting in a fast decay, while, on the other hand, larger crystal volumes free from defects exist, where excitons diffuse for a long time before meeting a trap site [52]. Consequently, the latter case will dominate the dynamics in the long term, successively prolonging the effective exciton lifetime as the decay proceeds.

Data fitting based on Eq. (2) indicated a good agreement of the diffusion model with the experiment during the first 100 ps. On a longer term, however, the fit approaches the baseline much faster than the data, suggesting the existence of a further species or contribution with a lifetime beyond the experimentally accessible time window of 1.9 ns. To describe this slow dynamics, we approximate this signature with a simple exponential decay with a lifetime τ_X. Moreover, we assume the contribution of this long-living component to scale linearly by a factor α with the amplitude A_0 of the excitonic contribution, i.e., with the exciton density, in accordance with the congruence of the time traces at different pump fluences. In summary, we obtain the following functional form for the transient signal:

$$\Delta A(t) = A_0\left[\exp(-Bt^{\frac{1}{2}}) + \alpha \exp\left(-\frac{t}{\tau_X}\right)\right],$$
$$B = c(n_t D)^{\frac{1}{2}}. \tag{3}$$

To test the potential influence of trap occupation, we additionally included the deactivation of traps during their occupation by subtracting the trapped excitons from the otherwise constant trap density n_t in Eq. (3). However, this fit resulted in a diverging n_t, which leaves the conclusion that the number of occupied defects remains negligible compared to the overall defects throughout the whole decay. Considering that the exciton densities of up to roughly 10^{14} cm^{-2} significantly exceed the reported defect densities in the range of 2×10^{10} to 3.5×10^{13} cm^{-2} for monolayer MoS_2 [21,24,25,54,55], a constant number of available or active traps only appears possible if occupied ones are rapidly depopulated again, i.e., if the trapped excitons recombine. Alternatively, the defects might function as traps irrespective of their occupation. Either way, even after catalyzing the recombination of an exciton, the defect can almost instantly function as a trap again; ergo the available or active defect density can be effectively treated as a constant.

The experimental data and the fit, as obtained from Eq. (3), match well for the monolayer flake, as shown in Fig. 5(b). We extracted a trapping rate constant of $B = 2.4 \times 10^5$ $s^{-\frac{1}{2}}$, which reflects the exciton diffusion coefficient and the trap density. Unfortunately, we are not aware of accurate measurements of exciton diffusion in mechanically exfoliated 1L MoS_2. Therefore, we estimate the exciton diffusion coefficient on the one hand to lie below the value of 3×10^{-1} cm^2 s^{-1} in WS_2 [50], where excitons are characterized by a lower effective mass than in MoS_2. On the other hand, due to higher effective carrier masses, the free carrier diffusion coefficient of 2.5×10^{-2} cm^2 s^{-1} for mono- and few-layer exfoliated MoS_2, as obtained from electrical mobility measurements on MoS_2 transistors [28,56], may be regarded as a lower limit for the excitonic value. From the range provided by these values, we estimate a trap areal density of about $n_t \approx 10^{10}$ cm^{-2}. This defect concentration lies slightly below the regime of reported values [21,24,25,54,55]. However, both diffusion and defects critically depend on experimental parameters such as the material, the sample thickness, and the preparation procedure.

Regarding the diffusion coefficient, studies on exciton and carrier diffusion in various monolayer and bulk TMDCs yielded a wide range of values. Many followed the approach

of monitoring the Gaussian width of the transient signal's spatial profile [20,27,57]. This method entails a potential major drawback, though, especially when merely a narrow wavelength regime is probed. Fluence-dependent spectral broadening effects as well as nonlinear recombination rates intrinsically cause a distortion of the initially excited Gaussian profile, drastically increasing the apparent diffusion coefficients with growing exciton density [50].

For the comparison of defect densities, similar problems arise. Generally, the amount of defects strongly varies with crystal quality and preparation method [54]. Moreover, the involvement as trapping states in the carrier or exciton dynamics may be limited to certain types of defects, representing merely a small fraction of their total number [24]. The energetic levels introduced by a defect may promote exciton recombination in particular for a certain kind of antisite or vacancy that accounts for only 1% of the overall defects [54]. This may cause the discrepancy between the trap concentration found in this work and the defect densities reported in other studies. Naturally, the multiplicity of parameters complicates the direct comparison of the obtained defect densities. Yet, the good agreement between fit and experimental data proves that the number of available defects does not change throughout the decay.

Besides the exciton diffusion, the fit additionally yields a small contribution of the exponential component around $\alpha = 7\%$ of the exciton amplitude A_0. The corresponding exponential lifetime of $\tau_X = 3.7$ ns should be regarded as no more than an indication for the rough time scale of this part of the dynamics, as the value already exceeds the observed temporal regime.

In principle, this long-living component may be attributed to trapped excitons, remaining free carriers that have not bound to form excitons, or thermal effects. In the former two cases, though, we would expect some variations of the temporal evolution of the signal with increasing pump fluence, caused by a limited availability of defects or a quadratic recombination rate equation, analogous to the bulk sample. As we do not observe this kind of fluence dependence, we exclude trapped excitons and remaining free carriers as the source of the long-term component. The latter option of thermal effects, in contrast, can indeed provide an explanation for the long-living signal. Laser irradiance is able to cause significant heating in MoS_2 monolayers, with the temperature increase depending roughly linearly on the applied excitation fluence [34]. With rising temperature, the absorption peaks are redshifted and broadened [58], causing transient signals similar to the observed ones. Finally, the heat dissipation to the substrate could happen on time scales comparable to the extracted exponential lifetime [34,59]. A detailed discussion of the impact and time regime of heating and cooling is presented in Sec. VI of the SM [36].

In total, our developed interpretation of the transient spectral signatures and their dynamics consistently describes measurements of other groups as well. Considering the work of Pogna *et al.* [22] and Vega-Mayoral *et al.* [24], their transient spectra of MoS_2 excited at 400 nm are consistent with an absorption redshift induced by localized species. On a picosecond time scale, the increased absorption peaks narrow, as explained by the thermalization of excited carriers. Afterwards, the spectra decay while retaining their shape, in agreement with our analysis of the recombination dynamics.

III. CONCLUSIONS

In this work, we conducted a comparative investigation of the transient dynamics in bulk versus monolayer MoS_2. We found the transient spectra to result from a redshift of the absorption bands based on local energy shifts in the environment of rather localized excited species. On top of that, the shifted absorption bands experience density-dependent collisional broadening due to Coulomb scattering of excited particles, especially in the monolayer.

Regarding the dynamics of the system, first, a thermalization of the excited carriers takes place on a subpicosecond time scale. In the monolayer, in addition, electrons and holes pair to form excitons in the course of this process. Second, the decay of the transient signal proceeds due to recombination processes. Here, the systematic variation of the excitation fluence allowed for the distinction between single- and multiparticle processes. In bulk MoS_2, we found a defect-assisted Auger recombination of electrons and holes, resulting in a decay rate depending superlinearly on the carrier densities. In the monolayer, on the contrary, we observed a diffusion-limited trapping of the excitons, with a linear influence of the exciton density in the rate equation.

All in all, we are able to resolve contradictions of the BGR model by introducing a localized nature of the excited species. Comparing bulk and monolayer MoS_2, we demonstrated the decisive impact of the different electronic properties, i.e., the band gap and the exciton binding energy, on the excited species dynamics. Notwithstanding, defects play an important role as trap states in the decay in thin as well as in thick flakes.

ACKNOWLEDGMENTS

The work was financially supported by the DFG via the Priority Program SPP 2102, "Light-controlled reactivity of metal complexes" (LO 714/11-1). T.V. thanks the University of Rostock for support via their Ph. D. Scholarship Program. T.K. gratefully acknowledges funding by the DFG via Grant No. KO 3612/4-1.

[1] T. Cheiwchanchamnangij and W. R. L. Lambrecht, Phys. Rev. B **85**, 205302 (2012).
[2] A. Chernikov, T. C. Berkelbach, H. M. Hill, A. Rigosi, Y. Li, O. B. Aslan, D. R. Reichman, M. S. Hybertsen, and T. F. Heinz, Phys. Rev. Lett. **113**, 076802 (2014).
[3] S. Lebègue and O. Eriksson, Phys. Rev. B **79**, 115409 (2009).
[4] D. Y. Qiu, F. H. da Jornada, and S. G. Louie, Phys. Rev. Lett. **111**, 216805 (2013).
[5] K. F. Mak, C. Lee, J. Hone, J. Shan, and T. F. Heinz, Phys. Rev. Lett. **105**, 136805 (2010).

[6] A. Splendiani, L. Sun, Y. Zhang, T. Li, J. Kim, C.-Y. Chim, G. Galli, and F. Wang, Nano Lett. **10**, 1271 (2010).

[7] K. F. Mak and J. Shan, Nat. Photonics **10**, 216 (2016).

[8] F. Withers, O. D. Pozo-Zamudio, A. Mishchenko, A. P. Rooney, A. Gholinia, K. Watanabe, T. Taniguchi, S. J. Haigh, A. K. Geim, A. I. Tartakovskii, and K. S. Novoselov, Nat. Mater. **14**, 301 (2015).

[9] H. S. Lee, S.-W. Min, Y.-G. Chang, M. K. Park, T. Nam, H. Kim, J. H. Kim, S. Ryu, and S. Im, Nano Lett. **12**, 3695 (2012).

[10] O. Lopez-Sanchez, D. Lembke, M. Kayci, A. Radenovic, and A. Kis, Nat. Nanotechnol. **8**, 497 (2013).

[11] M. Massicotte, P. Schmidt, F. Vialla, K. G. Schädler, A. Reserbat-Plantey, K. Watanabe, T. Taniguchi, K. J. Tielrooij, and F. H. L. Koppens, Nat. Nanotechnol. **11**, 42 (2015).

[12] A. Kudo and Y. Miseki, Chem. Soc. Rev. **38**, 253 (2009).

[13] D. Merki and X. Hu, Energy Environ. Sci. **4**, 3878 (2011).

[14] J. Ran, J. Zhang, J. Yu, M. Jaroniec, and S. Z. Qiao, Chem. Soc. Rev. **43**, 7787 (2014).

[15] Y. Zhu, Q. Ling, Y. Liu, H. Wang, and Y. Zhu, Phys. Chem. Chem. Phys. **17**, 933 (2015).

[16] T. Corrales-Sánchez, J. Ampurdanés, and A. Urakawa, Int. J. Hydrogen Energy **39**, 20837 (2014).

[17] M. Sarno and E. Ponticorvo, Int. J. Hydrogen Energy **44**, 4398 (2019).

[18] Y. Yu, S.-Y. Huang, Y. Li, S. N. Steinmann, W. Yang, and L. Cao, Nano Lett. **14**, 553 (2014).

[19] A. Chernikov, C. Ruppert, H. M. Hill, A. F. Rigosi, and T. F. Heinz, Nat. Photonics **9**, 466 (2015).

[20] Q. Cui, F. Ceballos, N. Kumar, and H. Zhao, ACS Nano **8**, 2970 (2014).

[21] P. D. Cunningham, K. M. McCreary, A. T. Hanbicki, M. Currie, B. T. Jonker, and L. M. Hayden, J. Phys. Chem. C **120**, 5819 (2016).

[22] E. A. A. Pogna, M. Marsili, D. De Fazio, S. Dal Conte, C. Manzoni, D. Sangalli, D. Yoon, A. Lombardo, A. C. Ferrari, A. Marini, G. Cerullo, and D. Prezzi, ACS Nano **10**, 1182 (2016).

[23] S. Sim, J. Park, J.-G. Song, C. In, Y.-S. Lee, H. Kim, and H. Choi, Phys. Rev. B **88**, 075434 (2013).

[24] V. Vega-Mayoral, T. Borzda, D. Vella, M. Prijatelj, E. A. A. Pogna, C. Backes, J. N. Coleman, G. Cerullo, D. Mihailovic, and C. Gadermaier, 2D Mater. **5**, 015011 (2017).

[25] H. Wang, C. Zhang, and F. Rana, Nano Lett. **15**, 339 (2014).

[26] H. Wang, C. Zhang, and F. Rana, Nano Lett. **15**, 8204 (2015).

[27] N. Kumar, J. He, D. He, Y. Wang, and H. Zhao, J. Appl. Phys. **113**, 133702 (2013).

[28] H. Shi, R. Yan, S. Bertolazzi, J. Brivio, B. Gao, A. Kis, D. Jena, H. G. Xing, and L. Huang, ACS Nano **7**, 1072 (2013).

[29] T. Völzer, M. Lütgens, F. Fennel, and S. Lochbrunner, J. Phys. B: At. Mol. Opt. Phys. **50**, 194003 (2017).

[30] U. Megerle, I. Pugliesi, C. Schriever, C. F. Sailer, and E. Riedle, Appl. Phys. B **96**, 215 (2009).

[31] A. Castellanos-Gomez, M. Buscema, R. Molenaar, V. Singh, L. Janssen, H. S. J. van der Zant, and G. A. Steele, 2D Mater. **1**, 011002 (2014).

[32] R. Frisenda, E. Navarro-Moratalla, P. Gant, D. P. D. Lara, P. Jarillo-Herrero, R. V. Gorbachev, and A. Castellanos-Gomez, Chem. Soc. Rev. **47**, 53 (2018).

[33] C. Hsu, R. Frisenda, R. Schmidt, A. Arora, S. M. Vasconcellos, R. Bratschitsch, H. S. J. van der Zant, and A. Castellanos-Gomez, Adv. Opt. Mater. **7**, 1900239 (2019).

[34] G. Plechinger, A. Castellanos-Gomez, M. Buscema, H. S. J. van der Zant, G. A. Steele, A. Kuc, T. Heine, C. Schüller, and T. Korn, 2D Mater. **2**, 015006 (2015).

[35] N. S. Taghavi, P. Gant, P. Huang, L. Niehues, R. Schmidt, S. M. de Vasconcellos, R. Bratschitsch, M. Garcá-Hernández, R. Frisenda, and A. Castellanos-Gomez, Nano Res. **12**, 1691 (2019).

[36] See Supplemental Material at http://link.aps.org/supplemental/10.1103/PhysRevB.103.045423 for sample preparation and characterization, details on the pump-probe setup, peak fitting, and a discussion of thermal effects on the transient spectra.

[37] K. P. Dhakal, D. L. Duong, J. Lee, H. Nam, M. Kim, M. Kan, Y. H. Lee, and J. Kim, Nanoscale **6**, 13028 (2014).

[38] R. Gillen and J. Maultzsch, IEEE J. Sel. Top. Quantum Electron. **23**, 219 (2017).

[39] P. Hein, A. Stange, K. Hanff, L. X. Yang, G. Rohde, K. Rossnagel, and M. Bauer, Phys. Rev. B **94**, 205406 (2016).

[40] Y. Li, J. Shi, Y. Mi, X. Sui, H. Xu, and X. Liu, J. Mater. Chem. C **7**, 4304 (2019).

[41] M. M. Ugeda, A. J. Bradley, S.-F. Shi, F. H. da Jornada, Y. Zhang, D. Y. Qiu, W. Ruan, S.-K. Mo, Z. Hussain, Z.-X. Shen, F. Wang, S. G. Louie, and M. F. Crommie, Nat. Mater. **13**, 1091 (2014).

[42] A. Steinhoff, M. Rösner, F. Jahnke, T. O. Wehling, and C. Gies, Nano Lett. **14**, 3743 (2014).

[43] T. Holstein, Ann. Phys. **8**, 325 (1959).

[44] M. Kang, S. W. Jung, W. J. Shin, Y. Sohn, S. H. Ryu, T. K. Kim, M. Hoesch, and K. S. Kim, Nat. Mater. **17**, 676 (2018).

[45] A. Thilagam, Physica B Condens. Matter **464**, 44 (2015).

[46] Z. Nie, R. Long, L. Sun, C. Huang, J. Zhang, Q. Xiong, D. W. Hewak, Z. Shen, O. Prezhdo, and Z. Loh, ACS Nano **8**, 10931 (2014).

[47] R. Wallauer, J. Reimann, N. Armbrust, J. Güdde, and U. Höfer, Appl. Phys. Lett. **109**, 162102 (2016).

[48] P. Steinleitner, P. Merkl, P. Nagler, J. Mornhinweg, C. Schüller, T. Korn, A. Chernikov, and R. Huber, Nano Lett. **17**, 1455 (2017).

[49] Y. Li, J. Shi, H. Chen, R. Wang, Y. Mi, C. Zhang, W. Du, S. Zhang, Z. Liu, Q. Zhang, X. Qiu, H. Xu, W. Liu, Y. Liu, and X. Liu, Nanoscale **10**, 17585 (2018).

[50] M. Kulig, J. Zipfel, P. Nagler, S. Blanter, C. Schüller, T. Korn, N. Paradiso, M. M. Glazov, and A. Chernikov, Phys. Rev. Lett. **120**, 207401 (2018).

[51] A. Singh, G. Moody, K. Tran, M. E. Scott, V. Overbeck, G. Berghäuser, J. Schaibley, E. J. Seifert, D. Pleskot, N. M. Gabor, J. Yan, D. G. Mandrus, M. Richter, E. Malic, X. Xu, and X. Li, Phys. Rev. B **93**, 041401(R) (2016).

[52] P. Grassberger and I. Procaccia, J. Chem. Phys. **77**, 6281 (1982).

[53] R. F. Kayser and J. B. Hubbard, Phys. Rev. Lett. **51**, 79 (1983).

[54] J. Hong, Z. Hu, M. Probert, K. Li, D. Lv, X. Yang, L. Gu, N. Mao, Q. Feng, L. Xie, J. Zhang, D. Wu, Z. Zhang, C. Jin, W. Ji, X. Zhang, J. Yuan, and Z. Zhang, Nat. Commun. **6**, 6293 (2015).

[55] H. Y. Jeong, S. Y. Lee, T. H. Ly, G. H. Han, H. Kim, H. Nam, Z. Jiong, B. G. Shin, S. J. Yun, J. Kim, U. J. Kim, S. Hwang, and Y. H. Lee, ACS Nano **10**, 770 (2016).

[56] B. Radisavljevic, A. Radenovic, J. Brivio, V. Giacometti, and A. Kis, Nat. Nanotechnol. **6**, 147 (2011).

[57] N. Kumar, Q. Cui, F. Ceballos, D. He, Y. Wang, and H. Zhao, Nanoscale **6**, 4915 (2014).

[58] E. Yalon, O. B. Aslan, K. K. H. Smithe, C. J. McClellan, S. V. Suryavanshi, F. Xiong, A. Sood, C. M Neumann, X. Xu, K. E. Goodson, T. F. Heinz, and E. Pop, ACS Appl. Mater. Interfaces **9**, 43013 (2017).

[59] S. V. Suryavanshi, A. J. Gabourie, A. B. Farimani, and E. Pop, J. Appl. Phys. **126**, 055107 (2019).